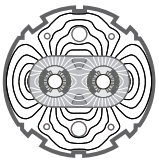

LHC Project Note 426

October 19, 2009
Yipeng.SUN@cern.ch

Impact of CMS Stray Field on the Large Hadron Collider Beam Dynamics and Thin Solenoid in the SixTrack Code

Y.-P. Sun, B. Auchmann, S. Fartoukh, M. Giovannozzi, S. Russenschuck, R. Tomás and F. Zimmermann

Keywords: solenoid, stray field, coupling, dynamic aperture

Summary

The impact of the CMS main solenoid field and stray field on the coupling and on the dynamic aperture is evaluated for both LHC collision (7 TeV) and injection optics (450 GeV). To study the impact of CMS solenoid field on the LHC dynamic aperture, a new element 'solenoid' has been added in the SixTrack code and debugged. In Appendix B and C the analytical formulae applied on the solenoid are presented.

1 Introduction

Measurements of the CMS solenoid stray field were performed on the right side of LHC IR5 (Interaction Region 5), by Mirko Pojer *et al.* [1]. It was found that at the interconnects of the triplets there could be a field leakage inside the beam pipe. Numerical simulations studied the detailed field distribution in this region, taking into account the cavern, the tunnel (armed concrete structure) and a rough model of the triplets.

In detail, the electromagnetic model in the ROXIE software [2] approximates the CMS solenoid by a 2D axisymmetric geometry, the axis of rotation being the solenoid axis. The geometrical data of the CMS iron yoke is taken from the CMS technical proposal [3]. The cavern walls, made of armored concrete, are modeled assuming a 10% iron content in volume. Moreover the model contains the ferromagnetic yokes of the inner-triplet magnets. Their geometry is taken from simplified drawings. The longitudinal position is given in the IR5 layout. Fig. 1 and Fig. 2 show the electromagnetic model, as well as the stray fields of the CMS solenoid in the region of the inner triplet magnets.

In Fig. 3 the simulated CMS solenoid main field is compared with an interpolation of the measurements [4] on the axis (center of beamline), with IP5 (Interaction Point 5) at the origin of the abscissa. A simple hard-edge model is used to describe the CMS field in

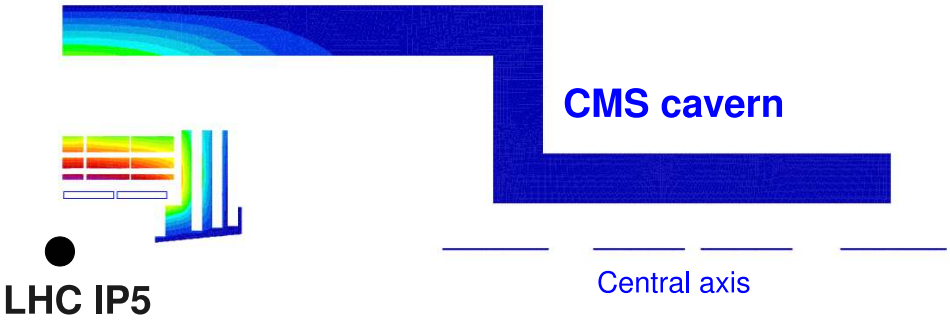

Figure 1: Magnetic vector potential in the ferromagnetic parts of the IR5 model.

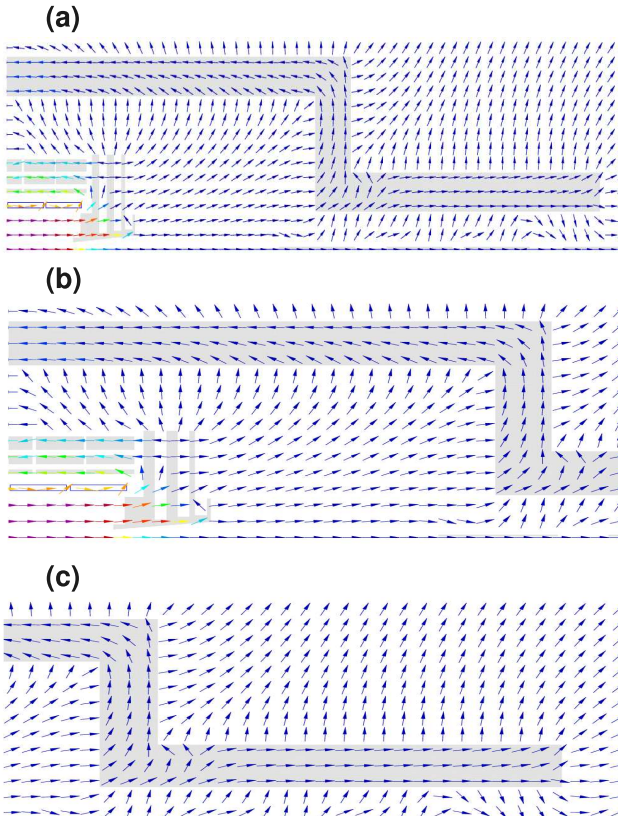

Figure 2: (a) Field vectors in the CMS cavern; (b) view of the cavern; (c) view of the inner triplet. The field model uses axial symmetry. The field strength is encoded in the color of the arrows, with a maximum field of about 4.2 T. Dark blue represents field strengths below 0.2 T.

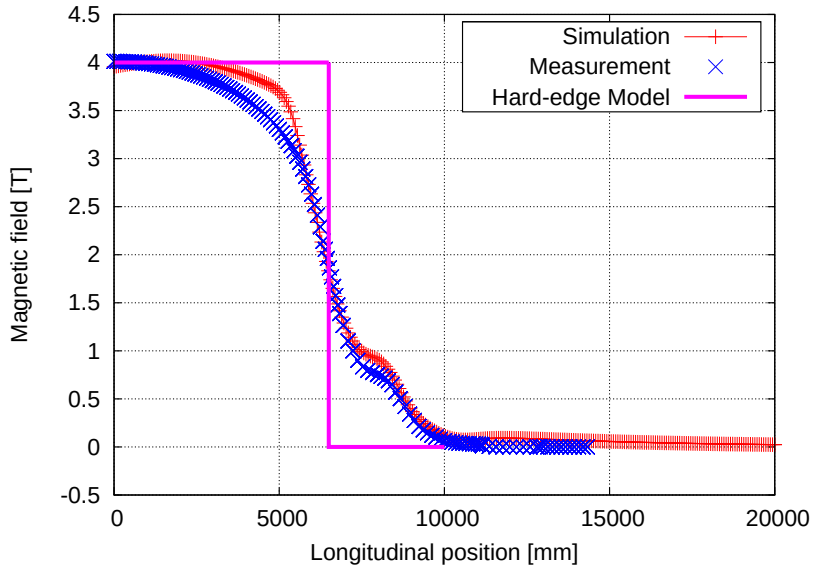

Figure 3: Comparison of CMS field between simulation and measurements [4]. IP5 is located at the origin of the abscisse. A simple hard-edge model is used (magenta lines).

subsequent particle tracking simulation, as shown by the magenta line in Fig. 3. A constant magnetic field of 4 T is considered and the magnetic length of CMS solenoid is assumed to be 11 m.

To extract the actual dependence of the radial component of the CMS solenoid stray field on the radial position r, a field matrix is defined between $r = 0$ mm and $r = 20$ mm with 11 points in radial direction and 500 points in axial direction (starting at 20 m from IP5). The range starts in front of the entrance of Q1, and ends after the exit of Q3 (55 m from IP5).

Values of the measured CMS stray field with a directional probe [1] are sketched in Fig. 4, while the simulated field, for the same region, is shown in Fig. 5. At the entrance of Q1, the longitudinal component is found to be around 25 mT in both cases. All in all, the simulated data are in reasonable agreement with the measurement.

2 Impact of CMS Solenoid

The longitudinal component B_s of the simulated CMS solenoid stray field is plotted in Fig. 6 (top), where we observe that except for the field on the axis, the longitudinal component is almost independent on r (0.5% difference at the most, as shown in Fig. 6 (bottom)). A similar hard-edge model is used to describe the stray field in the simulation and for each 'weak' solenoid the magnetic length is set to be 1 m.

The transverse component B_r of the simulated CMS solenoid stray field is plotted versus s in Fig. 7 (top), where we observe that the transverse component is different from zero only at the interconnects of the triplets quadrupoles (Q1, Q2 and Q3).

The transverse component of the CMS solenoid stray field is also plotted versus r at several specified longitudinal positions (interconnects of the triplets), as shown in Fig. 7 (bottom). To investigate the linearity of B_r, we calculate the deviation of the field with

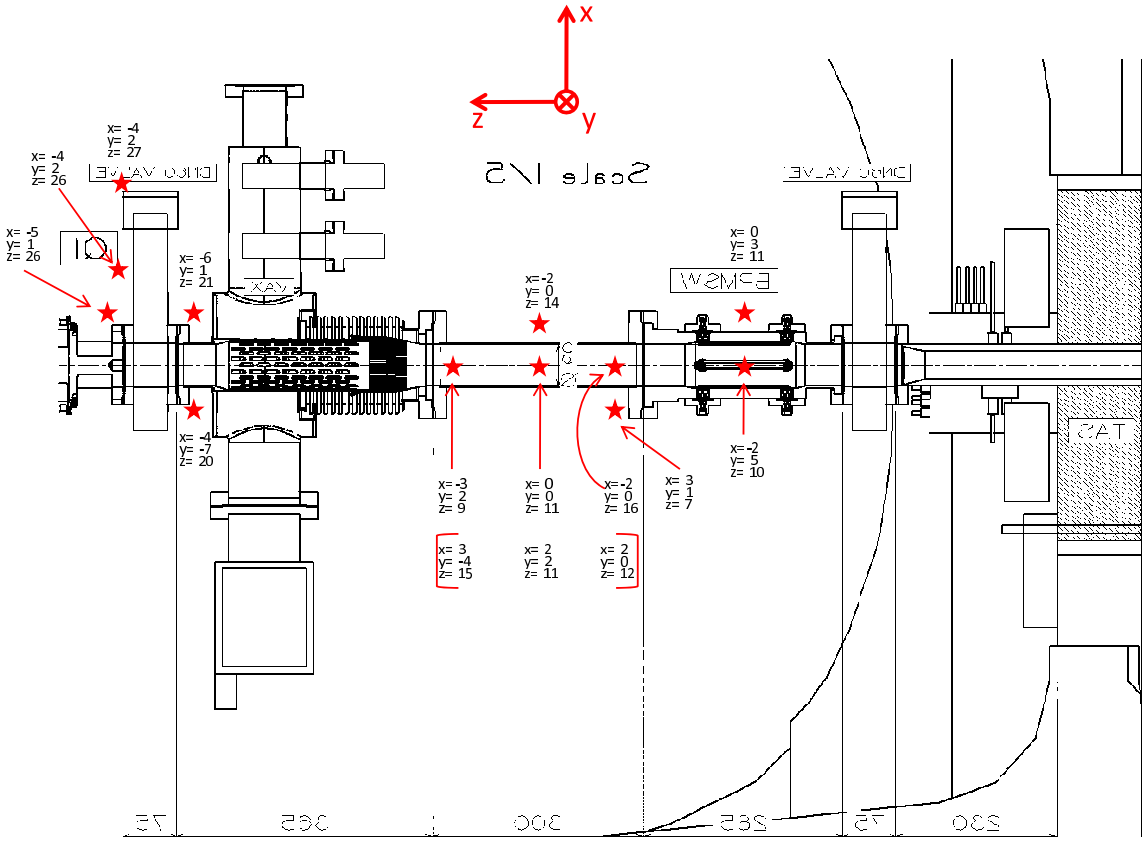

Figure 4: Measured CMS solenoid stray field from TAS (right) to entrance of Q1 (left), by Mirko Pojer *et al.* [1].

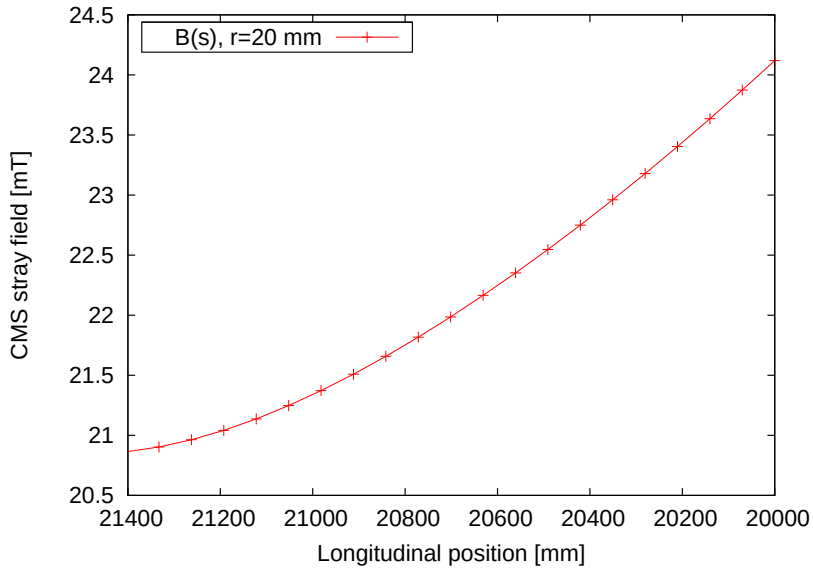

Figure 5: Longitudinal component of the CMS simulated stray field, from TAS (right) to entrance of Q1 (left) (to be compared with Fig. 4).

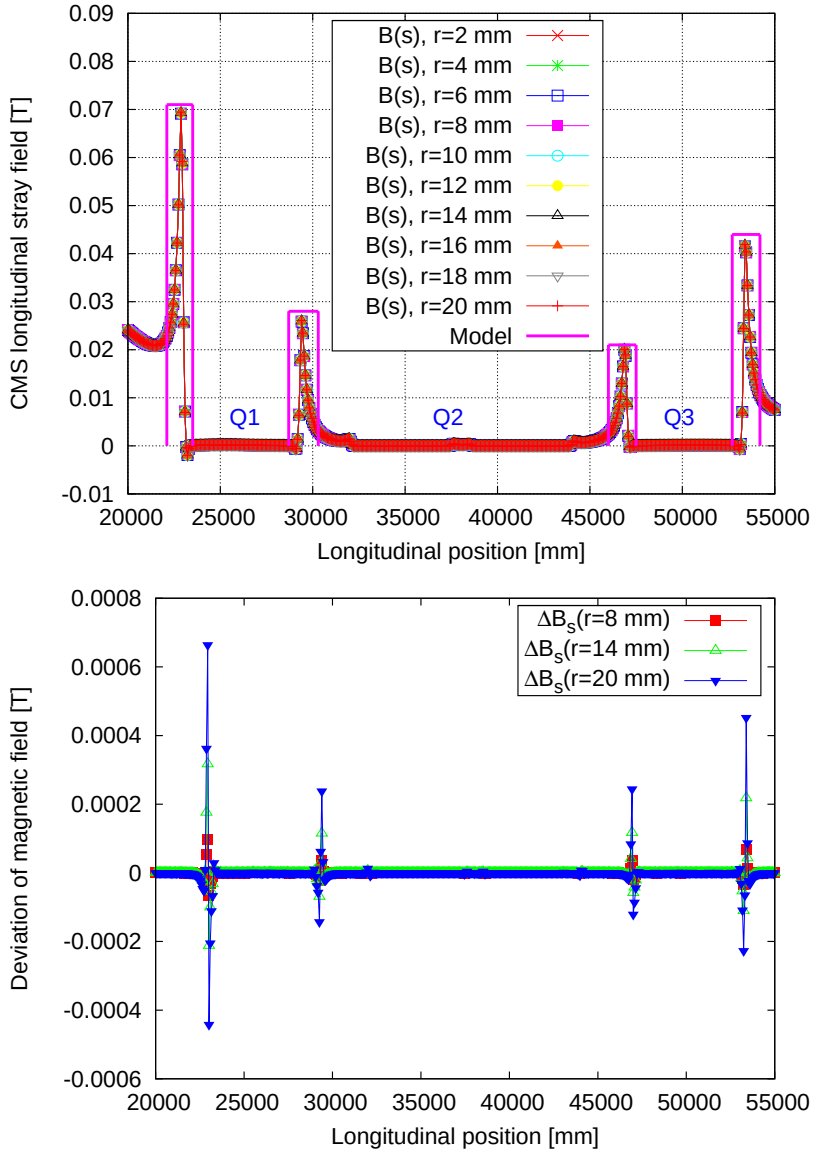

Figure 6: Longitudinal component of the CMS solenoid stray field (top), to describe which a simple hard-edge model is used (magenta lines) (the triplet locations are indicated). Deviation of the CMS longitudinal stray field (bottom), with respect to B_s at $r = 2$ mm.

respect to the linear case, $\Delta B_r = B_r(r) - \frac{dB_r}{dr}|_{r=2} \cdot r$, at different radial position r (2 mm, 4 mm, 6 mm,...20 mm). We find that it is very small and scales with r as an octupole-like component, as shown in Fig. 8. Taken the largest difference of the gradient 3.5×10^{-6} T/mm, this gives the largest nonlinearity of B_r as 6×10^{-5} T, at the reference radius of 17 mm, which is used to define the field quality of the LHC magnets. Given the tolerance of 1×10^{-4} T for the non-linear components of the triplets field, the transverse fringe field can be considered as linear in our simulations.

2.1 Coupling

Based on the simulation data of the CMS solenoid field, one main solenoid plus four 'weak' solenoids at each side of IP5 are used in the beam dynamic studies to model the CMS main and stray field, respectively. The coupling between horizontal and vertical motions, which is introduced by the solenoid is calculated by changing the strength of the arc focusing quadrupoles (QF), to obtain the tune split. A comparison of the betatron tune under several QF strengths is done between the results from MADX and SixTrack, as shown in Fig. 9, which proves that the solenoid recently implemented in SixTrack is equivalent to that in MADX.

As the impact of the solenoid on the beam is inversely proportional to the beam energy, it could have a larger coupling effect at LHC injection (the beta-function changes as well). That is confirmed by the results shown in Fig. 10. The coupling introduced by the CMS main field is found to be 2.99×10^{-4} at collision and 4.65×10^{-3} at injection. The CMS stray field has very tiny impact on the coupling, which leads to a coupling strength of 2.7×10^{-5} and 2.95×10^{-5} at collision and injection, respectively.

For the analytical estimation of the coupling strength from skew gradients and solenoids, the contributions to the coupling coefficients are (for the case $Q_x \mp Q_y = integer$) [5, 6]

$$C^{\mp} = \frac{1}{2\pi}\int_0^C \sqrt{\beta_x\beta_y}\left[K(s) + \frac{M(s)}{2}\left(\frac{\alpha_x}{\beta_x} - \frac{\alpha_y}{\beta_y}\right) - i\frac{M(s)}{2}\left(\frac{1}{\beta_x} \pm \frac{1}{\beta_y}\right)\right] e^{i(\mu_x(s)\mp\mu_y(s))}ds. \quad (1)$$

where $C^{\mp}$ denotes the coupling strength of the difference or sum resonance, C the circumference of the ring, β_x (β_y) the horizontal (vertical) beta function at the dedicated element (skew quadrupole or solenoid), α_x (α_y) the horizontal (vertical) alpha function at the dedicated element (skew quadrupole or solenoid), $\mu_x(s)$ ($\mu_y(s)$) the horizontal (vertical) phase advance at the dedicated element (skew quadrupole or solenoid).

Two important terms in the above formula are [6]

$$K(s) = \frac{1}{2}\frac{1}{B\rho}\left(\frac{\partial B_x}{\partial x} - \frac{\partial B_y}{\partial y}\right). \quad (2)$$

$$M(s) = \frac{1}{B\rho}B_s. \quad (3)$$

where $K(s)$ denotes the skew gradients (skew quadrupole, or nonlinear fringe field of solenoid), $M(s)$ the solenoid longitudinal field, and $B\rho$ the beam rigidity.

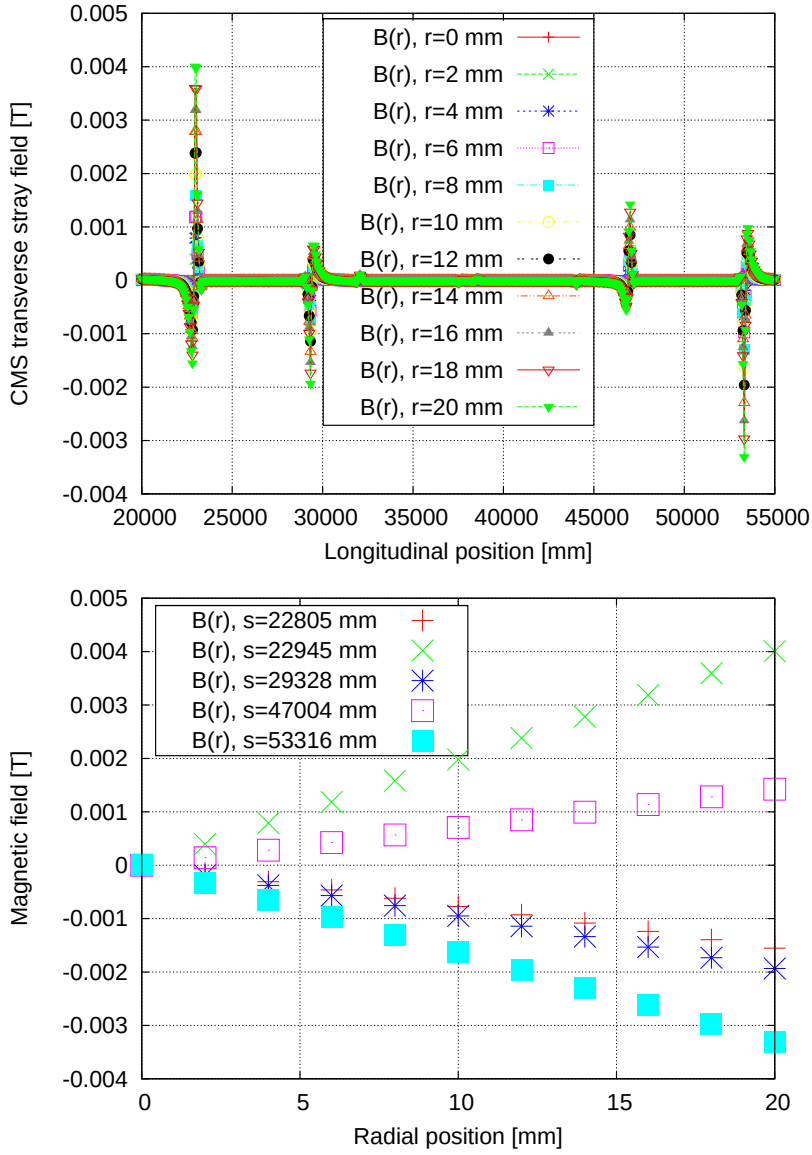

Figure 7: Transverse component of the CMS solenoid stray field (top). Transverse component of the CMS solenoid stray field at several specified longitudinal positions (interconnects of the triplets) (bottom).

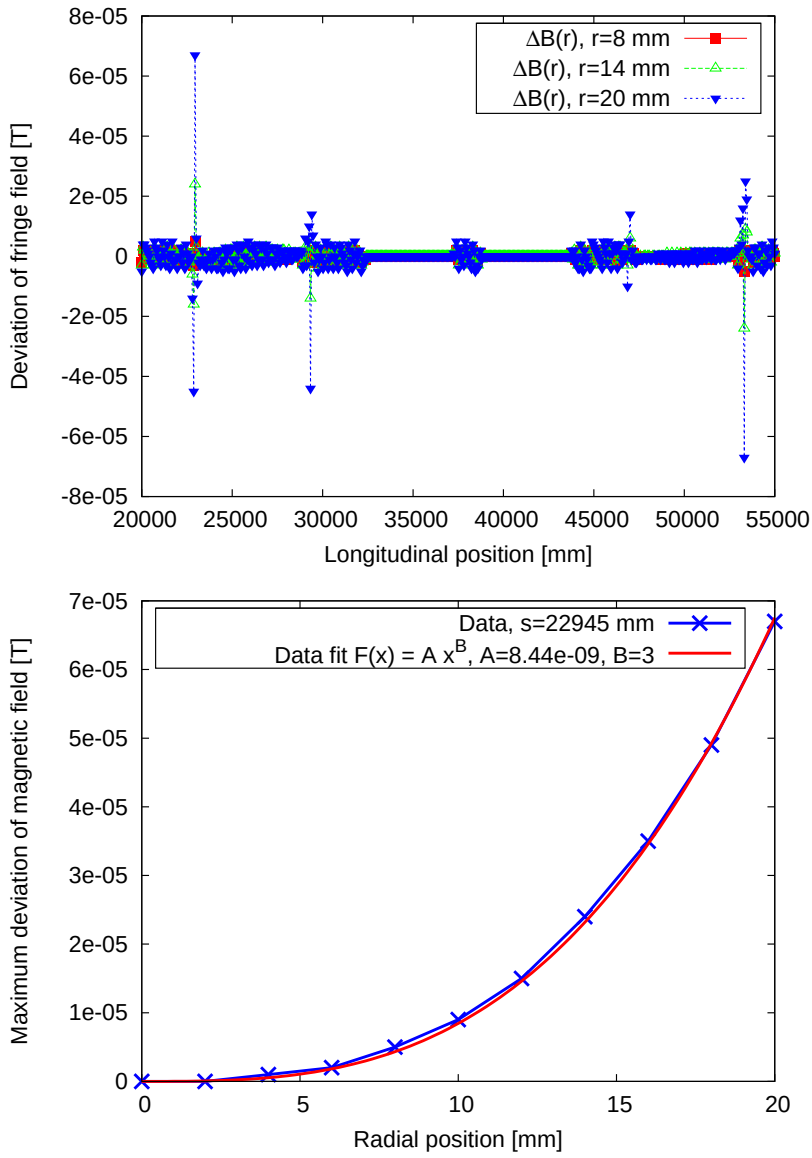

Figure 8: The deviation of the transverse fringe field $B_r(s, r)$ at different radial position r (8 mm, 14 mm, 20 mm), with respect to a linear approximation given by $\frac{dB_r}{dr}|_{r=2} \cdot r$ (top). Deviation of fringe field from linear approximation at s=22945 mm (bottom). The data fitting indicates that it is an octupole-like component.

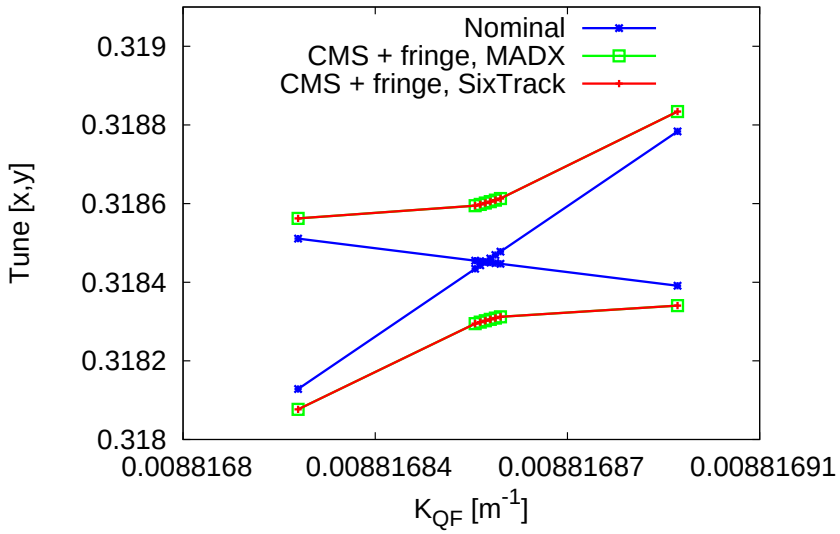

Figure 9: Comparison of the tune variation during a closest tune scan, between MADX and SixTrack, with CMS solenoid field.

We consider one pure solenoid located at the origin of the ring ($\mu_x(0) = \mu_y(0) = 0$). For the difference resonance case $Q_x - Q_y = integer$, the real part of C^- can then be simplified as (the linear fringe field of the solenoid generates $K(s) = 0$)

$$C_r^- = \frac{B_s L}{4\pi B\rho}\sqrt{\beta_x \beta_y}\left(\frac{\alpha_x}{\beta_x} - \frac{\alpha_y}{\beta_y}\right). \tag{4}$$

and the imaginary part of C^- becomes

$$C_i^- = -i\frac{B_s L}{4\pi B\rho}\sqrt{\beta_x \beta_y}\left(\frac{1}{\beta_x} + \frac{1}{\beta_y}\right). \tag{5}$$

where B_s denotes the longitudinal solenoid field, L the magnetic length of solenoid, β_x the horizontal beta function at the center of the solenoid, and β_y the vertical beta function at the center of the solenoid.

The total coupling is therefore [6]

$$C^- = \sqrt{C_r^{-2} + C_i^{-2}}. \tag{6}$$

The original optics functions without any solenoid fields (β, α and μ) at the CMS main solenoid and 8 'weak' solenoids (to describe the stray field) are listed in Table I and Table II, for LHC collision optics and injection optics, respectively. For each solenoid, assuming only this specified solenoid is present and that its center corresponds to the origin of the ring ($\mu_x(0) = \mu_y(0) = 0$), C_r^- and C_i^- are calculated and also listed in Table I and Table II, respectively.

For LHC at IP5 with round beams (difference resonance case $Q_x - Q_y = integer$) we have $\beta_x^* = \beta_y^*$, $\mu_x(0) - \mu_y(0) = integer$ and $\alpha_x = \alpha_y = 0$. By using formulae (4), (5) and (6), the coupling introduced by the CMS main field is calculated to be $C^- = C_i^- = 3 \times 10^{-4}$ at

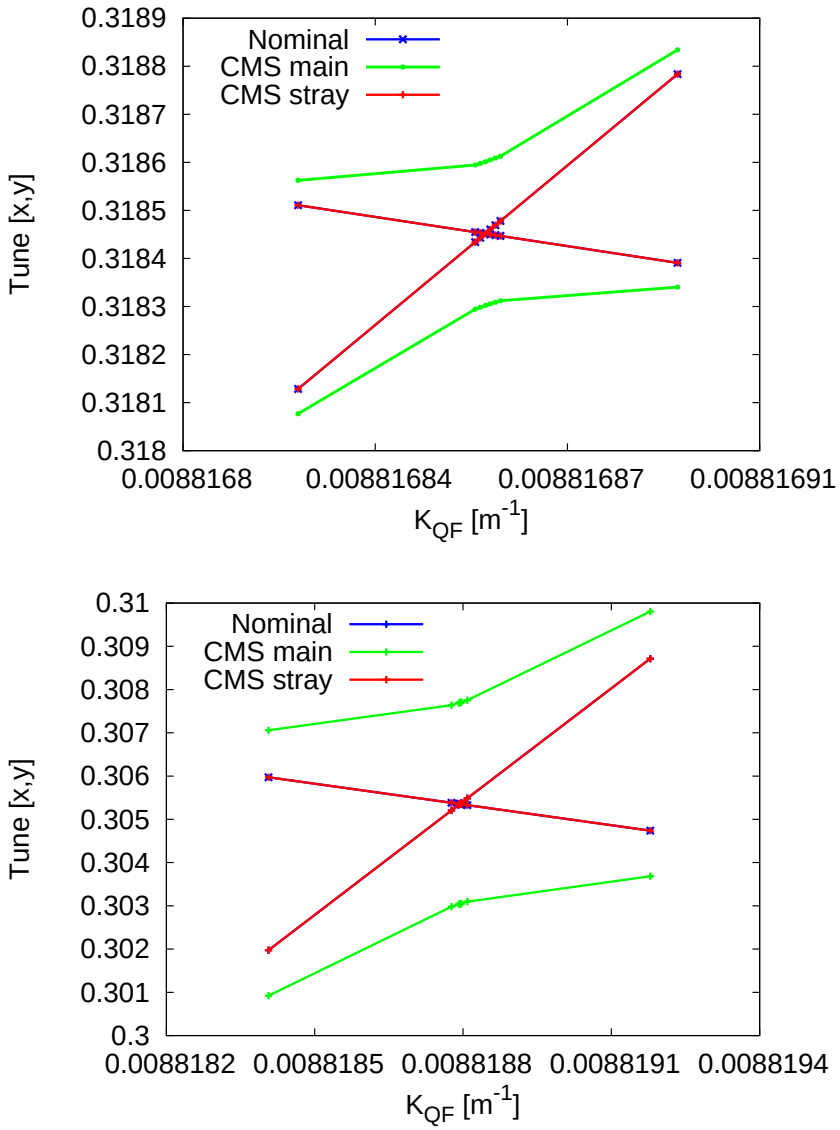

Figure 10: Coupling introduced by the CMS solenoid (MADX results), for the collision optics at 7 TeV (top) and for the injection optics at 450 GeV (bottom).

Table 1: Optics functions at the CMS main solenoid and 8 'weak' solenoids, LHC collision optics with origin at IP1.

Name	β_x [m]	β_y [m]	α_x	α_y	μ_x	μ_y	C_r^-	C_i^-[-i]
SOLECMS4L	1947	3890	-1.70	-25	31.81	29.35	-4e-06	2.7e-08
SOLECMS3L	3216	2444	-149	145	31.81	29.35	-7e-07	3.3e-08
SOLECMS2L	2825	1066	181	-16	31.81	29.36	1.4e-05	2.2e-07
SOLECMS1L	828	829	38	38	31.81	29.36	-7e-10	2.7e-07
IP5	0.55	0.55	0	0	32.05	29.60	0	3e-04
SOLECMS	0.55	0.55	0	0	32.05	29.60	0	3e-04
SOLECMS1R	828	829	-38	-38	32.30	29.85	6e-10	2.7e-07
SOLECMS2R	1065	2828	16	-181	32.30	29.85	1.4e-05	2.2e-07
SOLECMS3R	2441	3219	-145	149	32.30	29.85	-7.3e-07	3.3e-08
SOLECMS4R	3887	1948	25	1.71	32.30	29.85	-4e-06	2.7e-08

Table 2: Optics functions at the CMS main solenoid and 8 'weak' solenoids, LHC injection optics with origin at IP1.

Name	β_x [m]	β_y [m]	α_x	α_y	μ_x	μ_y	C_r^-	C_i^-[-i]
SOLECMS4L	105	197	-0.16	-1.22	31.83	29.36	-3.3e-06	4e-07
SOLECMS3L	176	125	-8.25	7.29	31.84	29.36	-5.5e-07	5e-07
SOLECMS2L	159	59	9.81	-1.18	31.85	29.40	1.25e-05	3.5e-06
SOLECMS1L	52	52	1.9	1.93	31.87	29.42	1.3e-08	4.2e-06
IP5	11	11	0	0	32.05	29.60	0	0.00466
SOLECMS	11	11	0	0	32.05	29.60	0	0.00466
SOLECMS1R	52	52	-1.94	-1.9	32.22	29.77	-1.4e-08	4.2e-06
SOLECMS2R	59	159	1.18	-9.78	32.25	29.79	1.26e-05	3.5e-06
SOLECMS3R	125	175	-7.31	8.23	32.28	29.80	-5.5e-07	5.3e-07
SOLECMS4R	198	105	1.23	0.16	32.29	29.81	-3.3e-06	4.2e-07

collision and $C^- = C_i^- = 4.66 \times 10^{-3}$ at injection, respectively, which agrees well with the tune split simulation. In this case, the coupling strength scales simply with energy.

By comparing Table I and Table II, we observe that α functions are comparatively small at the 8 'weak' solenoids for the LHC injection optics, and the main contribution to the coupling is from C_i. For the LHC collision optics, α function is very large (around 20 times larger than the injection case) at the second 'weak' solenoid 'SOLECMS2L' ('SOLECMS2R') and makes a large contribution to C_r, which is the main reason why the coupling introduced by the CMS stray field is similar at collision and injection (2.7×10^{-5} and 2.95×10^{-5}, respectively). To accurately calculate the coupling from all the solenoids, one has to apply the integration formula (1), with the appropriate factor $e^{i(\mu_x(s)\mp\mu_y(s))}$.

By using the LHC IR5 squeeze optics [7], and applying formulae (4) and (5), we calculate the coupling strength introduced by the CMS stray field at three beam energies (3.5 TeV, 5 TeV and 7 TeV). The coupling strength is shown in Fig. 11 versus β^*.

2.2 Dynamic aperture

The long-term dynamic aperture is determined by tracking particles with different initial coordinates in the SixTrack [8] code over 100,000 turns, which corresponds to 1/400 hour of real time. At the same time the short-term dynamic aperture is determined by tracking over 1000 turns. For this study the full range of the dynamic aperture search is set to be 20 σ, and the mesh size is 2 σ which is subdivided into 30 amplitude steps.

Concerning optics imperfections, the measured magnetic errors are included (both normal and skew multipole coefficients) up to a_{15} and b_{15} orders for all dipoles and quadrupoles. The corrections of the main dipole field errors by the b_3, b_4, and b_5 spool-piece families are taken into account. For collision the beam energy is 7 TeV and the nonlinear correctors in the triplets are used. The initial momentum offset is set to be 0.00027 (3/4 of the rf bucket; this corresponds to the standard convention for all LHC dynamic aperture studies). For injection the beam energy is 450 GeV and the initial momentum offset is set to be 0.00075.

From the minimum dynamic aperture over 60 seeds of the non-linear magnetic errors, which is shown in Fig. 12 (collision) and Fig. 13 (injection), we observe almost no impact from the CMS solenoid (main and stray field).

3 Solenoid in the code

3.1 MADX to SixTrack convertor

In the MADX code input file [9], the thin solenoid is defined as

label: SOLENOID, L=0, KS=real, KSI=real;

KS denotes the solenoid strength (unit radian/m), L the length of the solenoid and **KSI=KS*L** the solenoid integrated strength (unit radian). For a thin solenoid the length is always 0.

The solenoid strength **KS** can be calculated from the magnetic field

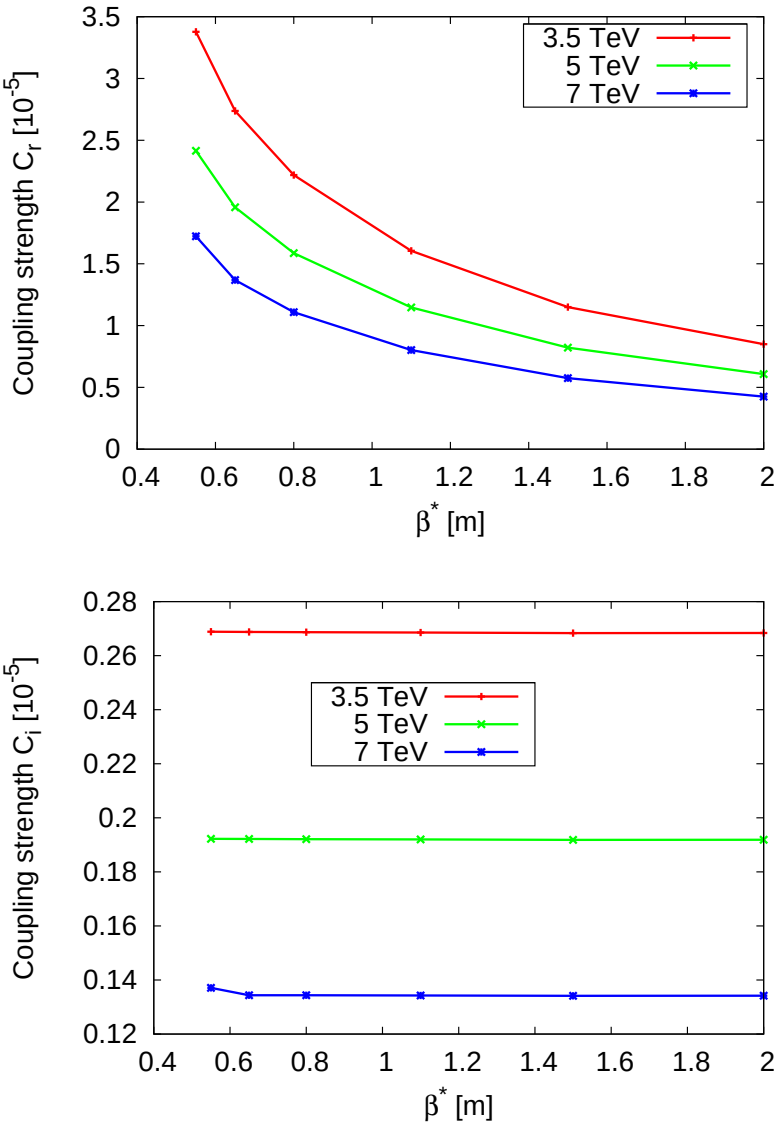

Figure 11: Coupling strength introduced by the CMS stray field at different energy versus β^* during squeeze. The contributions of the real part C_r and of the imaginary part C_i are shown on the left and on the right, respectively.

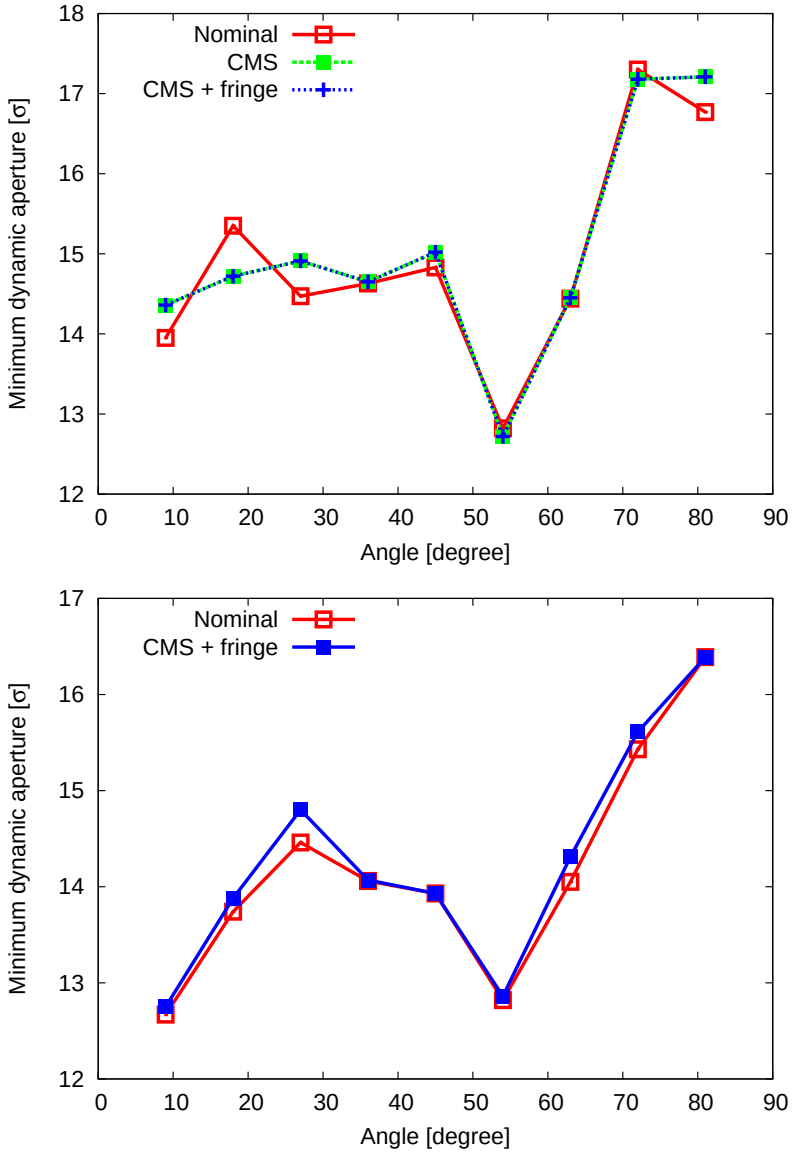

Figure 12: Minimum dynamic aperture over 60 seeds for nominal LHC optics, short term (1000 turns) (top) and long term (100,000 turns) (bottom). LHC collision optics at 7 TeV.

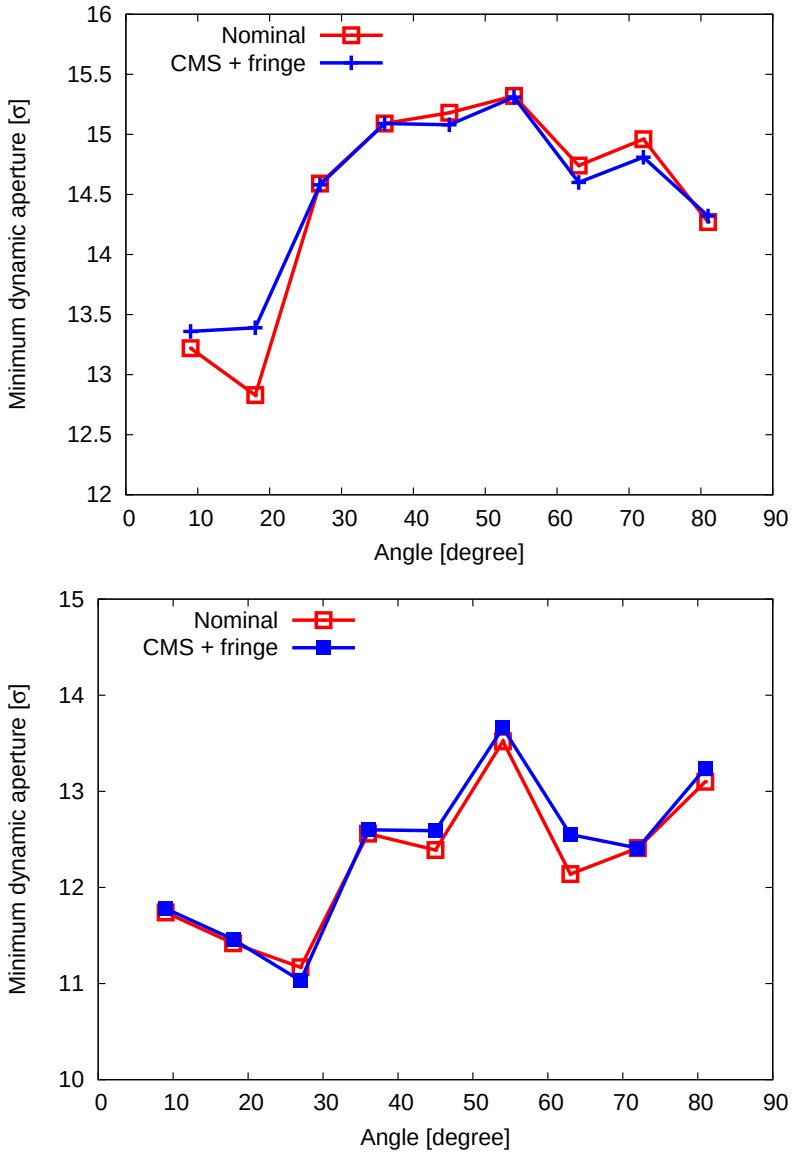

Figure 13: Minimum dynamic aperture over 60 seeds for nominal LHC optics, short term (1000 turns) (top) and long term (100,000 turns) (bottom). LHC injection optics at 450 GeV.

$$k_s = \frac{e}{p_s} \cdot B_s = \frac{B_s}{B\rho}. \tag{7}$$

where e denotes the particle charge, p_s the momentum, B_s the longitudinal magnetic field of solenoid, $B\rho$ the beam rigidity.

The MADX 'c6t' module is used to produce SixTrack [8] input files from an accelerator sequence which is described in MADX. A new element 'solenoid' is added in this module with the element type '25'. After the conversion, the solenoid appears in the SixTrack input file 'fort.2' (sequence) as

SOLENOID 25 KS KSI 0

3.2 SixTrack code

By applying Ripken's theory for the pure solenoid [10], and adding the formulae for solenoid fringe field which is presented in Appendix C, we introduced a new element 'Solenoid' in the SixTrack code [8]. This new element is implemented in the 8 tracking routines (4 dimensional and 6 dimensional), 2 differential algebra routines and 6 other routines (linear optics and resonances).

4 Conclusion

Comparison of the measured and simulated CMS stray field shows good agreement. The impact of the CMS solenoid field on the LHC beam dynamics was studied by simulation and by analytical estimation. The coupling introduced by the main field is 2.99×10^{-4} at collision and 4.65×10^{-3} at injection, which is acceptable [11]. The coupling introduced by the CMS stray field is similar at collision and injection (2.7×10^{-5} and 2.95×10^{-5}, respectively). A new element 'solenoid' has been defined in the MADX convertor and in the SixTrack code to perform tracking simulations. The dominant nonlinear field component of the solenoid stray field was shown to be octupole-like, and insignificant if compared with the tolerance criteria of the other multipoles of the triplet quadrupoles. There is almost no impact on the dynamic aperture from the CMS main and stray solenoid field. The orbit distortion from the combined effect of solenoid and the IP crossing scheme is not discussed in this paper.

The authors would like to thank B. Dalena for providing the interpolation data of the CMS measured field, M. Pojer and B. Bellesia for the measurements of the CMS stray field. The authors would also like to thank F. Schmidt for the cooperation work on the SixTrack code, and J. Barranco for the discussion on the SixTrack code.
This work was supported by the European Community-Research Infrastructure Activity under the FP6 "Structuring the European Research Area" programme (CARE, contract number RII3-CT-2003-506395), and under the FP7 "Capacities Specific Programme" (EuCARD, under Grant Agreement no 227579).

5 Appendix

5.1 Hamiltonian to describe the solenoid

If we rotate the transverse coordinates system by an angle ϕ, with the longitudinal coordinate unchanged, the Hamiltonian describing the solenoid should be invariant. The details are listed in Appendix A. The implication is that this Hamiltonian has cylindrical symmetry and that it is independent of the azimuthal coordinate in the cylindrical coordinates system.

In standard accelerator coordinates (canonical coordinates), the Hamiltonian to describe the pure solenoid is [10]

$$H_{sol} = \frac{1}{2} \cdot \left[(p_x + H \cdot y)^2 + (p_y - H \cdot x)^2 \right] \cdot \frac{P}{P_0}. \tag{8}$$

where H_{sol} denotes the Hamiltonian, p_x the horizontal momentum, p_y the vertical momentum, x the horizontal coordinate, y the vertical coordinate, P the momentum of any particle, P_0 the design momentum, and $H = 1/2 \cdot e/P_s \cdot B_s$.

If we rotate the transverse coordinates system by an angle ϕ, with the longitudinal coordinate unchanged, we have the new transverse coordinates as

$$x^{\phi} = x \cdot \cos\phi + y \cdot \sin\phi. \tag{9}$$

$$y^{\phi} = y \cdot \cos\phi - x \cdot \sin\phi. \tag{10}$$

$$p_x{}^{\phi} = p_x \cdot \cos\phi + p_y \cdot \sin\phi. \tag{11}$$

$$p_y{}^{\phi} = p_y \cdot \cos\phi - p_x \cdot \sin\phi. \tag{12}$$

By inserting formulae (9), (10), (11) and (12) into formula (8), we can prove that the Hamiltonian describing the solenoid is invariant under this rotation, as

$$\begin{aligned} H_{sol}^{\phi} &= \frac{1}{2} \cdot \left[(p_x{}^{\phi} + H \cdot y^{\phi})^2 + (p_y{}^{\phi} - H \cdot x^{\phi})^2 \right] \cdot \frac{P}{P_0} \\ &= \frac{1}{2} \cdot \left[(p_x + H \cdot y)^2 + (p_y - H \cdot x)^2 \right] \cdot \frac{P}{P_0} \\ &= H_{sol}. \end{aligned}$$

5.2 Ripken theory for solenoid

In thin-lens approximation, the solution for the canonical equations of motion is [10]

$$x^f = \hat{x}^f \cdot \cos\Delta\Theta + \hat{y}^f \cdot \sin\Delta\Theta. \tag{13}$$

$$p_x^f = \hat{p}_x^f \cdot \cos\Delta\Theta + \hat{p}_y^f \cdot \sin\Delta\Theta. \tag{14}$$

$$y^f = -\hat{x}^f \cdot \sin\Delta\Theta + \hat{y}^f \cdot \cos\Delta\Theta. \tag{15}$$

$$p_y^f = -\hat{p}_x^f \cdot \sin\Delta\Theta + \hat{p}_y^f \cdot \cos\Delta\Theta. \tag{16}$$

$$z^f = \hat{z}^f + \left[\hat{x}^f \cdot \hat{p}_y^f - \hat{y}^f \cdot \hat{p}_x^f\right] \cdot H(s_0) \cdot \Delta s \cdot \left(\frac{P}{P_0}\right)^2 \cdot \frac{v_0}{v}. \tag{17}$$

$$p_z^f = \hat{p}_z^f. \tag{18}$$

with

$$\Delta\Theta = H(s_0) \cdot \Delta s \cdot \frac{P}{P_0}. \tag{19}$$

where $(x^f, p_x^f, y^f, p_y^f, z^f, p_z^f)$ denote the final coordinates at the exit of the solenoid, $H(s_0)$ the solenoid strength, $H(s_0) \cdot \Delta s$ the solenoid integrated strength, v_0 the design velocity, v the velocity of any particle.

The coordinates $(\hat{x}^f, \hat{p}_x^f, \hat{y}^f, \hat{p}_y^f, \hat{z}^f, \hat{p}_z^f)$ can be obtained as [10]

$$\hat{x}^f = x^i. \tag{20}$$

$$\hat{p}_x^f = p_x^i - x^i \cdot [H(s_0)]^2 \cdot \Delta s \cdot \frac{P}{P_0}. \tag{21}$$

$$\hat{y}^f = y^i. \tag{22}$$

$$\hat{p}_y^f = p_y^i - y^i \cdot [H(s_0)]^2 \cdot \Delta s \cdot \frac{P}{P_0}. \tag{23}$$

$$\hat{z}^f = z^i - [H(s_0)]^2 \cdot \Delta s \cdot \frac{1}{2} \cdot \left[(x^i)^2 + (y^i)^2\right] \cdot \left(\frac{P}{P_0}\right)^2. \tag{24}$$

$$\hat{p}_z^f = p_z^i. \tag{25}$$

where $(x^i, p_x^i, y^i, p_y^i, z^i, p_z^i)$ denote the initial coordinates at the entrance of the solenoid.

In the SixTrack code a new thin element 'solenoid' is created (type 25), and formulae (13) to (25) are used to perform the coordinate transformation through this element.

5.3 Solenoid fringe field

For the transverse fringe field of the solenoid (linear case), from flux conservation in a hard-edge approximation, we find

$$B_r \cdot \Delta s = \frac{\Delta B_s}{2} \cdot r. \tag{26}$$

where B_r denotes the transverse fringe field of the solenoid, ΔB_s the change of the longitudinal solenoid field.

For a full serial expansion, one could use the formulae in [12].

At the entrance of the solenoid we have

$$\Delta p_x = \frac{e \cdot B_y \cdot \Delta s}{p_s} = \frac{e \cdot \Delta B_s}{2 \cdot p_s} \cdot y. \tag{27}$$

$$\Delta p_y = -\frac{e \cdot B_x \cdot \Delta s}{p_s} = -\frac{e \cdot \Delta B_s}{2 \cdot p_s} \cdot x. \tag{28}$$

At the exit of the solenoid we have

$$\Delta p_x = -\frac{e \cdot B_y \cdot \Delta s}{p_s} = -\frac{e \cdot \Delta B_s}{2 \cdot p_s} \cdot y. \tag{29}$$

$$\Delta p_y = \frac{e \cdot B_x \cdot \Delta s}{p_s} = \frac{e \cdot \Delta B_s}{2 \cdot p_s} \cdot x. \tag{30}$$

with

$$\frac{e}{p_s} = \frac{1}{B\rho}. \tag{31}$$

where e denotes the particle charge, p_s the momentum, $B\rho$ the beam rigidity.

References

[1] Summary notes of the CMS solenoid stray field, CERN/BE/ABP/LCU website.

[2] S. Russenschuck, in proceedings of EPAC08, page 2017-2019 (1998).

[3] M. Della Negra, CMS - The Compact Muon Solenoid, Technical Proposal, CERN/LHCC 94-38 (1994).

[4] B. Dalena, interpolation of the CMS measured field, private communication (2009).

[5] G. Guignard, the general theory of all sum and difference resonances in a three dimensional magnetic field in a synchrotron, CERN 76-06 (1976).

[6] CERN accelerator school proceedings, CERN 94-01, page 216, edited by S. Turner (1994).

[7] /afs/cern.ch/eng/lhc/optics/V6.503/IR5.

[8] F. Schmidt, CERN SL/94-56 (AP) (1994).

[9] MADX manual, http://mad.web.cern.ch/mad/.

[10] G. Ripken and F. Schmidt, CERN/SL/95-12 (AP), DESY 95-063 (1995).

[11] W. Herr, The Effects of Solenoids and Dipole Magnets of LHC Experiments, in proceedings of LHC Project Workshop CHAMONIX XV, 23-27 January 2006.

[12] Ph. Royer, PS/HP Note 99-12, Neutrino Factory Note 11 (1999).